Role of the P6−P3′ Region of the Serpin Reactive Loop in the Formation and Breakdown of the Inhibitory Complex†

Michael I. Plotnick,*,‡ Norman M. Schechter,§ Zhi Mei Wang,|| Xhuzuo Liu,|| and Harvey Rubin*,||

Pulmonary and Critical Care Division, Departments of Medicine, Dermatology, Biochemistry and Biophysics, and Microbiology, University of Pennsylvania, Philadelphia, Pennsylvania 19104

Received June 25, 1997; Revised Manuscript Received September 3, 1997⊗

ABSTRACT: Serpins have a large external peptide loop known as the reactive loop. Part of the reactive loop functions as the primary recognition site for target proteases; however, the complete role of the reactive loop in determining serpin specificity is unclear. In the current study, we investigated the reactive loop region that could potentially interact with the extended binding site of target proteases; the P6−P3′ region. We utilized a reactive loop switching strategy to determine the extent to which the inhibitory activity of α-1-protease inhibitor (PI) against human neutrophil elastase (HNE) could be transferred to α-1-antichymotrypsin (ACT), a serpin that does not inhibit HNE. A series of ACT−PI chimeras were constructed in which segments of increasing length taken from the P6−P3′ region of PI replaced the corresponding residues of ACT. The effectiveness of each chimera as an inhibitor of HNE was assessed by measuring (1) the rate of inhibitory complex formation and (2) the rate of complex breakdown (complex stability). Although all the ACT−PI chimeras were fully functional against chymotrypsin-like proteases, the series of chimeras showed no consistent progress toward the production of an inhibitor with the inhibitory properties of PI. The most rapid complex formation and most stable complexes were observed for chimeras with the P3−P1 residues of PI, whereas extending the replacement region to the P6 residue resulted in a considerable decrease in both inhibitory parameters. In order to study two additional features of the PI reactive loop that may play a role in the presentation of the P6−P3′ region to HNE, we constructed variants that contained a P4′ proline and deleted the P6′−P9′ residues. Changes on the prime side appeared to have little effect on rates of inhibition or complex stability. Overall, even the most effective chimeras demonstrated an inhibition rate constant at least 60-fold less than that observed for PI inhibition of HNE and the most long lived chimera−HNE complexes broke down more rapidly than PI−HNE complexes. These results indicate that residues in the reactive loop region predicted to contact a specific target protease cannot fully transfer inhibitory activity from one serpin to another, suggesting that specific reactive loop−serpin body and serpin body−protease body interactions play a significant role in determining serpin inhibitory activity against target proteases.

The wide variety of human serine proteases are regulated by proteins belonging to the serine protease inhibitor (serpin) family of proteins (*2*). Present understanding of the serpin mechanism of inhibition suggests that the serpin−protease complex is a covalent complex formed during the attempted substratelike hydrolysis of an exposed peptide loop at a specific site. This peptide loop, known as the reactive loop, ranges in size from approximately 20 to 25 residues in length, depending on the serpin, and generally presents a specific peptide bond (P1−P1′ bond[1]) to the target protease for hydrolysis. Multiple lines of evidence indicate that, for inhibition to occur, interaction of the P1 residue with the active site of a target protease must trigger a conformational change in the serpin. This conformational change involves insertion of the reactive loop into the A-β-sheet of the body of the serpin (*3*−*8*) and may be coupled to the distortion of the active site of the protease, which prevents the rapid completion of the catalysis (*9, 10*). The resulting serpin−protease complex is stable to dissociation by heat and SDS[2] and therefore is thought to contain a covalent bond between the Oγ of the active site serine of the protease and the carbonyl carbon of the P1 residue of the serpin. Evidence for P1−P1′ bond cleavage suggests that the serpin−protease complex exists as an acyl enzyme form (*11*, *12*). Although, the serpin−protease complex may appear stable for days, the protease slowly completes the hydrolysis of the serpin reactive loop, leading to an irreversibly inactivated serpin and active protease. The ultimate inactivation of the serpin defines the serpin mechanism of inhibition as a kinetic rather

† This work was supported by funding from the National Institutes of Health Grants HL-03495, HL-50523, AR-42931, and the Lexin Pharmaceutical Corp.

* Corresponding authors: Hospital of the University of Pennsylvania, 3400 Spruce St., Philadelphia, PA 19104. E-mail: mplotnic@mail.med.upenn.edu; rubinh@mail.med.upenn.edu.

‡ Pulmonary and Critical Care Division, Department of Medicine.

§ Departments of Dermatology and of Biochemistry and Biophysics.

|| Departments of Medicine and of Microbiology.

⊗ Abstract published in *Advance ACS Abstracts,* November 1, 1997.

[1] By convention, serpin reactive loop residue numbering is based on the nomenclature of Schechter and Berger (*1*) for substrates and proteases. Serpin P1−P1′ residues are the residues that border the scissile bond. Residues extending toward the N-terminus of the serpin are numbered P1, P2, P3, ..., P*n* and residues extending toward the C-terminus are numbered P1′, P2′, P3′, ..., P*n*′. The corresponding binding sites on the protease are numbered S*n*, ..., S3, S2, S1, S1′, S2′, ..., S*n*′.

[2] Abbreviations: ACT, α-1-antichymotrypsin; rACT, recombinant α-1-antichymotrypsin; PI, α-1-protease inhibitor; HNE, human neutrophil elastase; SI, stoichiometry of inhibition; CMK, chloro methyl ketone; SDS−PAGE, sodium dodecyl sulfate−polyacrylamide gel electrophoresis; DTT, dithiothreitol.

S0006-2960(97)01530-4 CCC: $14.00

than a thermodynamic process and differentiates serpins from the standard mechanism inhibitors. The serpin inhibitory reaction can therefore be viewed as proceeding in two stages: the rapid formation of the inhibitory complex and the slow breakdown of the complex to inactive serpin and active protease.

The role of reactive loop residues in determining the rate of complex formation and complex breakdown is not entirely clear. We previously demonstrated that replacing the P1 or the P3−P3′ residues of recombinant ACT with the corresponding residues of HNE inhibiting serpin, PI, converted ACT from a substrate to an inhibitor of HNE (*13*). The P3−P3′ region variant, rACT−P3P3′, inhibited HNE with a greater second-order inhibition constant, k_{inh}, than the P1 variant, rACT−L358M. In addition, rACT−P3P3′−HNE complexes broke down more slowly than rACT−L358M−HNE complexes; i.e., HNE formed more stable complexes with rACT−P3P3′ than rACT−L358M. These results suggested that reactive loop residues other than P1−P1′ may be important in complex formation and stabilization by virtue of their interaction with the extended substrate binding site of HNE. However, k_{inh} of rACT−P3P3′ for HNE remained almost 2 orders of magnitude less than the k_{inh} of PI for HNE, and rACT−P3P3′−HNE complexes did not obtain the stability of PI−HNE complexes. Therefore, this work also demonstrated that the P3−P3′ region of the reactive loop of PI contained some but not all of the structural determinants for inhibitory activity against HNE.

In the following report, we describe our continued investigation on the role of the PI reactive loop in determining inhibitory activity against HNE. Evidence that the substrate binding surface of HNE may make contact with residues extending from P6 to P3′ (*14*−*16*) suggests that the P3−P3′ residues studied previously may only represent a subset of the reactive loop residues that constitute the contact region between PI and HNE. Therefore, we investigated the HNE inhibitory activity of ACT−PI chimeras with the P6−P3′ region of PI replacing the corresponding residues of ACT. We also studied the effect on HNE inhibitory activity of two features of the PI reactive loop which may play a role in the presentation of the contact residues to HNE. These features include (1) the presence of a proline residue at P4′ and (2) the absence of four residues that correspond to the P6′−P9′ of ACT (i.e., the PI reactive loop is four residues shorter than ACT on the prime side).

MATERIALS AND METHODS

Materials. HNE was obtained from CalBiochem and TLCK-treated bovine pancreatic α-chymotrypsin (chymotrypsin) was from Worthington. PI was from Miles (Prolastin). Substrates and N-MeO-Suc-AAPV-CMK were from Bachem. *n*-Dodecyl β-D-maltoside (dodecyl maltoside) was from Anatrace. Standard protein markers for SDS−PAGE gels were from Enprotech.

Construction, Expression, and Purification of rACT−PI Chimeras. The construction of the ACT expression vector pACT and the purification of recombinant ACT have been described previously (*13*, *17*). Briefly, most of the variants were produced by site-directed mutagenesis of pACT using an overlap−extension PCR method. For historical reasons, rACTcas−P3P3′, rACTcas−LeuP3P3′, and rACTcas−P3P4′ΔP6′9′ were produced using cassette mutagenesis and a vector with a *Kpn*I restriction site created at the position corresponding to P10−P9 and an *Mlu*I restriction site created at P10′−P11′. Introduction of these restriction sites changed the reactive loop sequence at P10−P9 from Ala−Ala to Gly−Thr and changed P10′−Val to Thr. In our experience, there are no major differences in the inhibitory properties of ACT variants prepared with the cassette and pACT vectors (*13*). Oligonucleotides were produced by the Oligonucleotide Synthesis facility at the Wistar Institute, Philadelphia, PA.

Determination of Protease Concentrations. Chymotrypsin concentration was determined assuming a specific activity of 3.0 μmol of product (nmol of chymotrypsin)$^{-1}$ min^{-1} measured under standard chymotrypsin assay conditions: 0.4 M Tris, pH 8.0, 1.8 M NaCl, 1 mM Suc-AAPF-*p*-nitroanilide (substrate), and 9% DMSO. This value represents the mean of multiple chymotrypsin solutions that underwent active site titration with *N*-*trans*-cinnamoylimidazole (*18*). HNE concentrations were determined by assuming a specific activity of 0.6 μmol of product (nmol of HNE)$^{-1}$ min^{-1} measured under standard HNE assay conditions: 0.1 M HEPES, pH 7.5, 0.5 M NaCl, 1 mM MeO-Suc-AAPV-*p*-nitroanilide (substrate), and 9% DMSO. The specific activity was determined by active site titration of HNE with PI (*13*). The concentration of *p*-nitroaniline formed was determined using a molar extinction coefficient at 410 nm of 8800 cm^{-1} M^{-1}.

Determination of Inhibitor Concentrations/Inhibitor Activity. The concentration of active PI in stock solutions was estimated by titration of a known solution of chymotrypsin, assuming an SI of 1 (*13*). The concentration of ACT−PI chimera preparations was also determined using chymotrypsin. All exhibited an SI of 1 using an $A^{1\%}$ at 280 nm of 10 cm^{-1} to estimate ACT concentration in titrations. The $A^{1\%}$ at 280 nm was established for wild-type rACT preparations that were characterized as completely active by SDS−PAGE analysis; i.e., preparations that demonstrated stoichiometric formation of the high molecular weight complex with chymotrypsin. Thus, the SI of 1 determined for all the chimeras indicated that the recombinants were close to 100% active.

Titrations Studies. Determination of the Stoichiometry of Inhibition for HNE. Titrations of HNE activity by ACT−PI chimeras were performed in 25−100 μL of buffer containing 0.1 M Tris, pH 8.0, 0.1 M NaCl, and 0.01% dodecyl maltoside (HNE titration buffer). Reactions contained a constant concentration of HNE (typically between 0.5 and 2.0 μM) and varying concentrations of purified inhibitor. Incubation times were adjusted so that complex breakdown would not influence the measurement of SI. Residual HNE activity was determined by diluting an aliquot of the reaction mixture into 0.5 mL of standard HNE assay buffer and measuring the rate of substrate hydrolysis over 1 min. The SI was determined by regression analysis of the dependence of residual HNE activity on $[I]_0$:$[E]_0$.

Studies To Determine the Second-Order Inhibition Rate Constants k_{inh}. The inhibition rate constant for the reaction of HNE and PI was determined under second-order conditions as described previously (*13*). Inhibition rate constants for the reaction of HNE and ACT−PI chimeras were determined in the presence of substrate and under pseudo-first-order conditions with $[I]_0$:$[E]_0$ at least 10-fold the SI. The assay buffer utilized for these experiments consisted of 0.1 M HEPES, pH 7.5, 0.1 M NaCl, 0.01% dodecyl

maltoside, and 9% DMSO (rate assay buffer). Progress curves were monitored for 10−15 min. k_{obs}, the apparent first-order rate constant in the presence of substrate was determined by nonlinear fit of the progress curve data to eq 1, which is a relationship derived for irreversible inhibition

$$A(t) = V_i(1 - e^{-k_{obs}t})/k_{obs} + A_0 \quad (1)$$

(*19*). $A(t)$ is the A_{410nm} of the substrate measured at time (t). V_i and A_0 values obtained from fits correspond to the initial enzyme rate of substrate hydrolysis and the A_{410nm} at time zero, respectively. The second-order inhibition rate constant, k_{inh}, was calculated using the relationship in eq 2. k'_{obs} is the

$$k_{inh}[I]_0 = k'_{obs} = k_{obs}(K_m + [S])/K_m \quad (2)$$

pseudo-first-order inhibition rate constant corrected for the presence of substrate, [S] is the substrate concentration, and K_m is the Michaelis constant. A K_m of 0.15 mM was determined for the hydrolysis of MeO-Suc-AAPV-*p*-nitroanilide by HNE under the reaction conditions employed. Experiments were performed with either 0.5 or 1.0 mM substrate. Several reactions demonstrated a nonzero residual rate which was attributed to breakdown of the complex during the measurement (see below) and not to reversible dissociation of the complex. In these cases, reactions were performed with $[I]_0$ so that the residual rate was <10% of the initial rate.

Studies To Determine the Rate Constant for Complex Breakdown, k_{bkdn}. The rate constant for the breakdown of serpin−HNE complexes was determined by following the return of HNE activity with time. The reaction buffers used 0.1 M Tris, pH 8.0, and 0.01% dodecyl maltoside, with either 0.1 or 0.4 M NaCl. High-salt buffer was usually used in studies with inhibitors that formed long-lived complexes (hours) with HNE. Complexes were formed at high HNE concentrations, 0.5−2 μM, so that complex formation did not overlap with breakdown. $[I]_0$:$[E]_0$ ratios were chosen such that at least 50% of the protease formed complex. Residual HNE activity was measured for aliquots removed at designated times as described for titrations. Loss of HNE activity in parallel (uninhibited) controls was minimal. In most cases, controls revealed less than 10% loss of activity, although up to 20% loss of activity was occasionally noted when experiments lasted for >12 h. In such cases, the HNE activity of the reaction was normalized to the HNE activity of the control at the corresponding time point. The first-order rate constant for complex breakdown, k_{bkdn}, was determined by nonlinear fit of HNE activity versus time data to a single-exponential function, eq 3, where V_f was the control HNE activity.

$$V(t) = V_f - (V_f - V_i)e^{-(k_{bkdn}t)} \quad (3)$$

SDS−PAGE Analysis. rACT variants were incubated with HNE as described for the above titration studies. Reactions were stopped at the appropriate time by the addition of 200 μM (final concentration) N-MeO-Suc-AAPV-CMK to inhibit any free elastase. Denaturing buffer with 2% SDS and 20 mM DTT (final) was then added, and samples were heated at 100 °C for 6 min. Proteins were resolved on 10−12% minigels in Tris-glycine buffer using a BioRad MiniProteanII device. Coomasie Brilliant Blue R250 was used for visualizing protein bands.

Table 1: Reactive Loop Sequences for ACT, ACT−PI Chimeras, and PI[a]

inhibitor	reactive loop
	358
	P15 P6 P1 P1′ P5′ P10′
ACT	GTEASAATAVKITL**L**SALVETRTIV
rACTcas	GT T
rACT-L358M	**M**
rACT-P2P3′	P**M**SIP
rACT-P3P2′	IP**M**SI
rACT-P3P3′	IP**M**SIP
rACTcas-P3P3′	GT IP**M**SIP T
rACTcas-LeuP3P3′	GT IP**L**SIP T
rACT-P3P4′	IP**M**SIPP
rACTcas-P3P4′ΔP6′9′	GT IP**M**SIPP ----T
rACT-P4P3′	AIP**M**SIP
rACT-P6P3′	LEAIP**M**SIP
PI	GTEAAGAMFLEAIP**M**SIPPE----V

[a] rACTcas, rACT−L358M, rACT−P3P3′, and rACTcas−P3P3′ were previously described by Rubin et al. (*13*).

Determination of Reactive Loop HNE Cleavage Sites by Matrix-Assisted Laser Desorption (MALD) Mass Spectroscopy. The sequence of the C-terminal peptide fragments generated by cleavage of recombinant serpins by HNE were determined by MALD mass spectroscopy. ACT−PI chimeras and HNE were incubated in titration buffer with $[I]_0$ approximately 10 μM. Incubation times and reaction stoichiometries were chosen so that the products of reactive loop cleavage were generated in sufficient concentration to be detected by mass spectroscopy but represented primary cleavage sites. Aliquots were removed at predetermined times and the reaction stopped in the aliquot with 200 μM N-MeO-Suc-AAPV-CMK. SDS−PAGE analysis was performed on a sample from each time point to determine which aliquots would be submitted for mass spectroscopic analysis. Unless otherwise indicated, aliquots with <50% of the serpin cleaved or complexed to HNE were chosen in order to minimize second reactive loop cleavages. These aliquots were frozen in liquid nitrogen and stored at −70 °C until analyzed.

RESULTS

The amino acid sequences of the P10−P10′ region of the serpins studied are shown in Table 1. The interaction of HNE with ACT−PI chimeric variants exhibited behavior best characterized by assuming two consecutive irreversible reactions: inhibition by formation of the SDS-stable complex and subsequent breakdown of this complex to release free HNE and cleaved-inactive serpin. These processes were evaluated for each chimera by determining the rate constants for inhibition, k_{inh}, and complex breakdown, k_{bkdn}. The values for these rate constants as well as the stoichiometry of inhibition for the serpin−HNE reactions are presented in Table 2 and Table 3.

Inhibition Rate Constants. k_{inh} for the inhibition of HNE by the ACT−PI chimeras was determined under pseudo-first-order conditions by the analysis of progress curves (see Materials and Methods). k_{inh} values for the series of variants with reactive loop switches covering the region of the loop likely to contact the extended-substrate binding site of HNE are presented in Table 2. In contrast to our expectations, rACT−P6P3′, the inhibitor with the greatest loop switch,

Table 2: Kinetic and Stoichiometric Parameters for the Reaction of HNE with ACT, P6−P3′ Region Chimeras, and PI

		$k_{inh} \times 10^{-4}$	$k_{bkdn} \times 10^5$ (s^{-1})	
	SI	(M^{-1} s^{-1})	0.1 M NaCl	0.4 M NaCl
rACT	substrate[a]			
rACT−L358M	5[a]	4[a]	10	20
rACT−P2P3′	2.5	3[b]	20	
rACT−P3P3′	1.4[a]	10[a]	0.7	3
rACT−P4P3′	1.8	6[c]	50	
rACT−P6P3′	<2	0.4[d]	70	
PI	1	600[e]		nd[f]

[a] Data were taken fom Rubin et al. (*13*). [b] $[E]_0$ = 15 nM, $[I]_0$ = 0.9−1.3 μM. [c] $[E]_0$ = 15 nM, $[I]_0$ = 0.4−1.8 μM. [d] $[E]_0$ = 7−20 nM, $[I]_0$ = 7.2 μM. [e] Determined under second-order conditions ($[E]_0$ = $[I]_0$ = 7.5 nM). [f] No detectable HNE release after 48 h in 0.8 M NaCl.

Table 3: Kinetic and Stoichiometric Parameters for the Reaction of HNE with P3PX′ Chimeras

		$k_{inh} \times 10^{-4}$	$k_{bkdn} \times 10^5$ (s^{-1})	
	SI	(M^{-1} s^{-1})	0.1 M NaCl	0.4 M NaCl
rACT−P3P2′	1.4	6		3
rACT−P3P4′	1.3	10		3
rACTcas−P3P3′	1.4[c]	10	0.9	6
rACTcas−P3P4′ΔP6′9′	1.2	4	1	5

[a] $[E]_0$ = 15 nM, $[I]_0$ = 0.2−0.6 μM. [b] $[E]_0$ = 15 nM, $[I]_0$ = 0.1−0.8 μM. [c] Data taken from Rubin et al. (*13*). [d] $[E]_0$ = 7−14 nM, $[I]_0$ = 0.5−1.5 μM.

demonstrated the lowest k_{inh} for HNE of 4×10^3 M^{-1} s^{-1}. k_{inh} for the other chimeras fell within a narrow range of 3×10^4 to 1×10^5 M^{-1} s^{-1}, with rACT−P3P3′ demonstrating the greatest inhibition rate constant. The highest rate constant obtained for any of the ACT−PI chimeras remained almost 2 orders of magnitude lower than k_{inh} for HNE by wild-type PI. This series of ACT−PI chimeras failed to attain the k_{inh} observed for the inhibition of HNE by PI and failed to demonstrate a progressive improvement in k_{inh} with contact region switches of increasing size. Therefore, it appears that replacement of the sequence of the P6−P3′ region of ACT alone is not sufficient to attain the rapid inhibition rate constant of PI for HNE.

We next considered whether the inhibitory activity of ACT−PI chimeras might more fully recapitulate the activity of wild-type PI if the reactive loop switches incorporated not only the contact region residues of PI but two additional features unique to the PI reactive loop. These features are the relatively large number of Pro residues (P2, P3′, P4′) in close proximity to the P1−P1′ bond and the shorter length of the PI reactive loop (four residues shorter than the ACT loop). In order to investigate the role of these features in determining the inhibition rate constant against HNE, a second series of ACT−PI chimeras (Table 3) were produced that contained (1) only the P2 Pro residue (rACT−P3P2′), (2) all three Pro residues (rACT−P3P4′), and (3) all three residues as well as the deletion of the P6′−P9′ residues (rACTcas−P3P4′ΔP6′9′). The chimeras in the Table 3 series were constructed with the P3−P1 residues of PI since the analysis of the first series of chimeras suggested that this sequence change appeared to produce the most potent HNE inhibitors. However, analysis of the P3PX′-type chimeras demonstrated that the addition of Pro residues and the shortening of the reactive loop had little effect on inhibition rates. k_{inh} values fell in essentially the same narrow range of 4×10^4 to 1×10^5 M^{-1} s^{-1} that was obtained for the

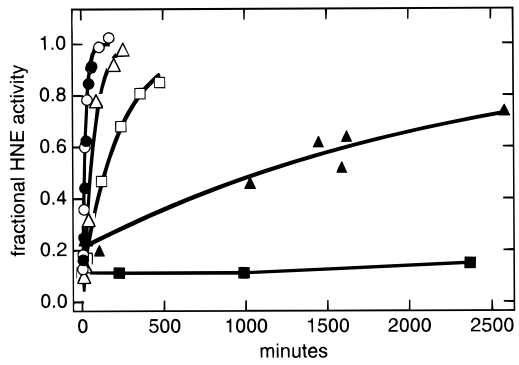

FIGURE 1: Time course for the release of HNE from serpin−HNE complexes. Fractional HNE activity in each reaction mixture is plotted as a function of time for reactions of HNE with (●) rACT−P6P3′ ($[I]_0$:$[E]_0$ = 3), (○) rACT−P4P3′ ($[I]_0$:$[E]_0$ = 1.5), (△) rACT−P2P3′ ($[I]_0$:$[E]_0$ = 2.5), (□) rACT−L358M ($[I]_0$:$[E]_0$ = 3), (▲) rACT−P3P3′ ($[I]_0$:$[E]_0$ = 1), and (■) PI reactions ($[I]_0$:$[E]_0$ = 0.9). Fractional activity was determined by comparison of residual HNE activity in reactions to the HNE activity of uninhibited controls at the corresponding time points. Lines through data points represent nonlinear fits of data to a first order process.

Table 2 series. Therefore, the failure of the residues of the P6−P3′ region of PI to completely transfer the inhibitory activity of PI to ACT appears to be due to additional factors external to the reactive loop.

Complex Stability. The stability of the serpin−HNE complexes was assessed in experiments in which the release of active HNE from complexes was followed over time. Since HNE release occurs at the same concentration and buffer conditions at which the complex was formed, i.e., without dilution of the complex, these analyses measure serpin turnover rather than the dissociation of a reversible complex. It has been shown previously that the rate of complex breakdown is increased at higher NaCl (and sodium phosphate) concentrations (*13*, *20*). The mechanism accounting for this effect has not been delineated. For practical reasons, chimeras that formed the most stable complexes with HNE were studied under high NaCl conditions (0.4 M). The increased rate of complex breakdown that occurred under these conditions allowed for the determination of k_{bkdn} without having to correct for significant nonspecific loss of HNE activity in controls followed over long incubation times.

Analysis of complex stability for the P6−P3′ region chimeras demonstrated abrupt changes in the rates of chimera−HNE complex breakdown, rather than a progressive increase in complex stability, as successively larger portions of the PI contact region were incorporated in the chimeras (Table 2 and Figure 1). rACT−P3P3′ formed complexes with HNE that were considerably more stable than those formed by the other P6−P3′ region chimeras. While rACT−P3P3′−HNE complexes released active HNE with a half-life that exceeded 20 h in 0.1 M NaCl, rACT−P2P3′, rACT−P4P3′, and rACT−P6P3′ formed complexes with HNE that broke down with a half-life that was less than 1 h. rACT−L358M−HNE complexes broke down with a half-life of approximately 2 h.

Breakdown rates for complexes of P3PX′-type chimeras (including rACT−P3P3′) with HNE were measured under high-salt conditions for the reasons discussed above. Analysis of these k_{bkdn} values revealed that P3PX′ chimeras form complexes with HNE that are considerably more stable than the complexes formed by any of the other reactive loop

chimeras. P3PX′ chimera−HNE complexes breakdown more slowly in high-salt buffer than do other chimera−HNE complexes in standard (0.1 M) salt buffer (compare Table 2 and Table 3). In addition, analysis of k_{bkdn} values for P3PX′ chimera−HNE complexes suggested that changes on the prime side of the reactive loop did not appear to affect complex stability, even when the P6′−P9′ residues were deleted; compare k_{bkdn} values for rACTcas−P3P3′ with rACTcas−P3P4′ΔP6′9′. However, no ACT−PI chimera formed complexes with HNE that were as stable as those formed by PI. Even in buffer containing 0.8 M NaCl, which increases k_{bkdn} of chimera−HNE complexes to values even greater than reported for 0.4 M NaCl, there was no demonstrable breakdown of PI−HNE complexes after incubation for 48 h (see Figure 1).

SDS−PAGE analysis of the interaction of HNE with the ACT−PI chimeras demonstrated that all the chimeras form the characteristic SDS-stable complex. Furthermore, there was qualitative agreement between SDS-stable complex formation and inhibition of hydrolytic activity. These results suggest that despite the relative short life span of some of the chimera−HNE complexes, the interaction between these serpins and HNE reflects the general serpin mechanism of inhibition. Figure 2A demonstrates one such analysis for the interaction of rACT−P6P3′ with HNE. The formation and breakdown of the characteristic SDS-stable complex as well as the corresponding turnover of the inhibitor are reflected by (1) the initial increase and subsequent decrease in the complex band (C), (2) the progressive decrease in the native inhibitor band (I), and (3) the progressive increase in the modified (cleaved) inhibitor band (I^c).

Stoichiometry of Inhibition. The requirement for a stoichiometric excess of inhibitor to completely inhibit a target protease is the result of substratelike interactions that lead to rapid hydrolysis of the reactive loop and serpin inactivation rather than formation of the inhibitory complex. Such reactive loop hydrolysis may occur at P1−P1′ or at another site (*13*, *21*). Titrations of HNE with ACT−PI chimeras demonstrated SI values that ranged from 1.2 to 5 (Tables 2 and 3). The SI for rACT−P6P3′ is reported as <2.0 because titration curves were nonlinear even with $[E]_0$ of 1 μM (see Figure 3A). This is the result of complex breakdown occurring at the same time as complex formation. Panels B and C of Figure 3 show titrations of HNE with rACT−P2P3′ and rACT−P4P3′, two variants for which linear titrations could be obtained despite the relatively low stability of the complexes.

SDS−PAGE analysis of titration reactions of HNE with these as well as the P3PX′ variants demonstrated qualitative agreement with the stoichiometry of complex formation obtained from titrations, indicating that the SI was indeed the result of competing inhibitory and substratelike reactions. Figure 2B is an example of one such SDS−PAGE analysis, the titration of HNE by rACT−P4P3′. $[E]_0$ was held constant and $[I]_0$ was varied as in the titration reactions. The relative densities of the bands corresponding to complexes (C and C^c) and cleaved serpin (I^c) reflect the SI of 1.8 reported in Table 2. Bands corresponding to intact inhibitor (I) are seen in lanes 5 and 6, where $[I]_0$ exceeds SI × $[E]_0$. In addition, the complete loss of the HNE band is observed in these lanes.

It had been previously shown (*13*) by N-terminal analysis that rACT−L358M is cleaved by HNE not only at the P1−P1′ site but at the P6−P5 and P4−P3 sites as well. The

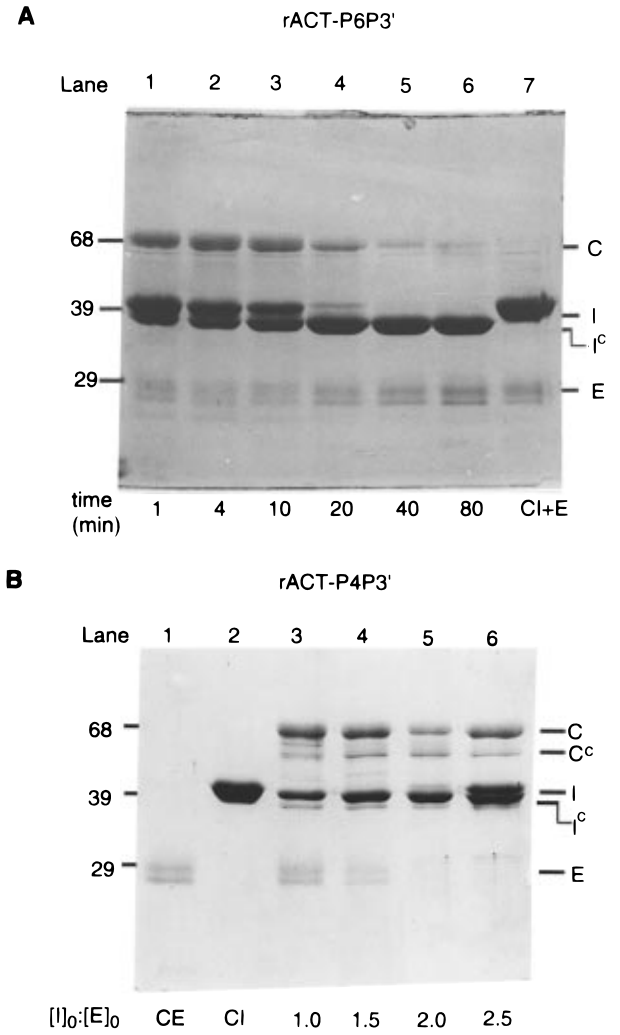

FIGURE 2: SDS−PAGE analysis of ACT−PI chimera−HNE reactions. (A) rACT−P6P3′−HNE time course experiment. rACT−P6P3′ was reacted with HNE at room temperature in HNE titration buffer (0.1 M NaCl) and $[I]_0$:$[E]_0$ = 10 μM:3 μM. Aliquots were removed at designated times and 200 μM (final) N-MeO-Suc-AAPV-CMK (final) was added. After 1 min, samples were denatured as described in Materials and Methods. Incubation times are indicated on bottom of gel. CI+E indicates that lane 7 contains control HNE and inhibitor; HNE was inhibited with N-MeO-Suc-AAPV-CMK prior to addition of the serpin. Numbers on the left side of the gel indicate the position of standard molecular weight markers. On the right side of the gel, the position of native inhibitor, cleaved inhibitor, complex, and HNE are indicated by I, I^c, C, and E, respectively. (B) rACT−P4P3′−HNE titration experiment. $[E]_0$ = 2.6 μM was held constant and $[I]_0$ varied. Reaction volume was 20 μL prior to addition of denaturing buffer. CE at the bottom of lane 1 indicates that the lane contains only HNE. CI at the bottom of lane 2 indicates that this lane contains only rACT−P4P3′ (4.4 μM). The molar ratio ($[I]_0$:$[E]_0$) of rACT−P4P3′ to HNE is denoted on the bottom of the gel for lanes 3−6. N-MeO-Suc-AAPV-CMK was added to all reactions (including controls) after a 1 min incubation and then prepared as described in Materials and Methods. The position of native inhibitor, cleaved inhibitor, complex, cleaved complex, and HNE are indicated by I, I^c, C, C^c, and E, respectively.

requirement for a 4-fold excess of rACT−Met to inhibit HNE was determined to largely result from the P6−P5 and P4−P3 cleavages. rACT−P3P3′ was shown to be cleaved at the P6−P5 but not at the P4−P3 site. Cleavage site analysis by mass spectroscopy of the ACT−PI chimeras produced for the current investigation established that HNE cleaves all the chimeras at P6−P5 except rACT−P6P3′ (see Table 4). Therefore, the SI values for all chimeras except rACT−

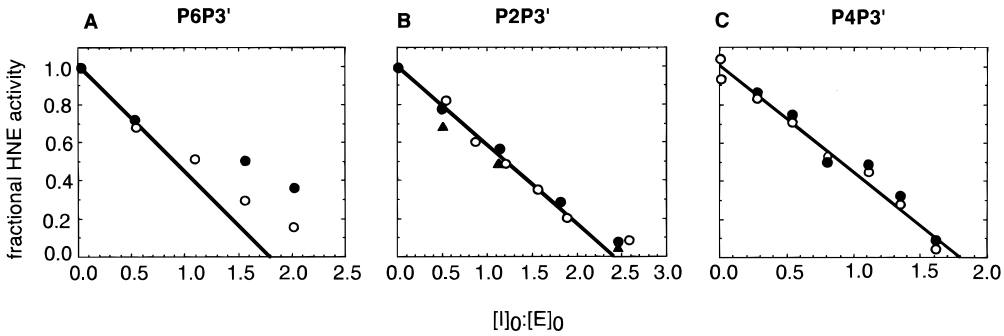

FIGURE 3: Titration of HNE with ACT−PI chimeras. (A) titration of HNE with rACT−P6P3′: $[E]_0 = 1.6\ \mu M$; (○) 5 min incubation; (●) 30 min incubation. (B) Titration of HNE with rACT−P2P3′: (○) $[E]_0 = 1.6\ \mu M$, 15 min incubation; (●) $[E]_0 = 800$ nM, 15 min incubation; (▲) $[E]_0 = 800$ nM, 25 min incubation. (C) Titration of HNE with rACT−P4P3′: $[E]_0 = 280$ nM; (○) 2 min incubation; (●) 5 min incubation.

Table 4: Mass of C-Terminal Peptide Fragments Detected by MALD Mass Spectroscopy of Chimera−HNE Reactions

		cleavage site[a]	
serpin	P6−P5 actual (calc)[b]	P1−P1′ actual (calc)	P4′−P5′ actual (calc)
rACT−P2P3′	5226 (5222)[c]	4654 (4652)	4257 (4255)[c]
rACT−P4P3′	5198 (5192)[c]	4656 (4652)	4254 (4255)[c]
rACT−P6P3′	nd[d]	4654 (4652)	4257 (4255)
rACTcas−P3P4′ΔP6′9′	4762 (4763)	4180 (4177)	nd[d]
rACTcas−LeuP3P3′[e]	5216 (5218)	4653 (4652)	4256 (4257)

[a] Cleavage of the reactive loop at these sites was inferred from the masses detected. [b] Actual, mass detected; calc, calculated mass for fragments released from ACT. [c] The P6−P5 fragment was observed when the reaction was stopped with <20% of the rACT variant cleaved or complexed. The P4′-P5′ fragment was observed when approximately 80% serpin was cleaved or complexed. Prime side cleavages are thought to represent second cleavages. [d] Not detected. [e] Fragments consistent with P6′−P7′, P10′−P11′, and P11′−P12′ cleavage were also detected.

P6P3′ could be attributed, at least in part, to cleavage at site(s) other than P1−P1′. Furthermore, since the SI could not clearly be attributed to a suicide substratelike mechanism, we did not report k_{inh} values normalized for SI (*17*, *22*, *23*).

Effect of the P1 Residue on ACT−HNE Complexes. Wild-type ACT is rapidly turned over by HNE even though HNE appears to interact with the Leu residue at P1. We previously demonstrated that replacing the P1−Leu with a Met residue (rACT−L358M) converts ACT to an inhibitor of HNE. In the present study, we found that the residues at the P3 and P4 positions may, in part, determine complex stability. We therefore considered the possibility that a Met residue at the P1 site is able to stabilize complexes between ACT and HNE to a greater extent than a Leu residue. In order to further investigate the effect of the P1 residue on ACT−HNE complex stability, a P1 revertant of rACTcas−P3P3′ (rACTcas−LeuP3P3′) was produced. This construct was chosen because it placed a P1−Leu in the context of an ACT−PI chimera that formed relatively long lived complexes. Analysis of the inhibitory activity of rACTcas−LeuP3P3′ against HNE demonstrated extremely transient inhibition. Complex breakdown was so rapid that during titration experiments HNE activity increased steadily upon dilution of the reaction mixtures in assay buffer with a 50% return of HNE activity occurring after approximately 1 min. As a result, dependable values for SI and kinetic constants could not be obtained. However, an SDS-stable complex could be demonstrated and cleavage site analysis confirmed that the P1−Leu was recognized by HNE along with the P6−P5 cleavage site (Table 4). While we were unable to quantify the relative effect on k_{bkdn} of a P1−Leu versus a P1−Met residue, the finding of transient inhibition does, in fact, suggest that a Leu residue in the P1 position of ACT is less able to stabilize the complex with HNE than a Met residue.

DISCUSSION

Although much progress has been made in understanding the serpin mechanism of inhibition in general, there is still only a rudimentary knowledge of the structural elements that determine the activity of serpins against specific target proteases. Investigations of a number of serpin−protease interactions have demonstrated that reactive loop residues near P1−P1′ can influence complex formation or inhibition (*19*, *24*−*30*). These studies suggest that reactive loop residues throughout the region predicted to interact with the extended substrate binding site of the target protease may play an important role in determining the inhibitory activity of serpins. In the current study, we examine the extent to which both inhibition rate and complex stability for the reaction of PI with HNE are determined by the sequence of the P6−P3′ region, the putative contact region for HNE. Variants of ACT, which is essentially a substrate for HNE, were constructed with residues from the P6−P3′ region of PI, replacing the corresponding residues in ACT. These ACT−PI chimeras were then evaluated with respect to HNE inhibitory activity. Although some of the ACT−PI chimeras were potent inhibitors of HNE, even the most efficient chimeras demonstrated a k_{inh} for HNE 60-fold lower than PI and even the most stable chimera−HNE complexes demonstrated a k_{bkdn} considerably more rapid than PI−HNE complexes. These results indicate that the contact region sequence is not the sole determinant of serpin specificity.

The relatively slow HNE inhibition rates observed for the ACT−PI chimeras indicate that features of the reactive loop and/or body of PI essential for a rapid HNE inhibition rate were not incorporated in the P6−P3′ region chimeras. We previously demonstrated that the charge arrangement of ACT does not preclude ACT−PI chimeras from attaining high inhibition rates against HNE (*13*). In the current study, we considered the possibility that differences in the k_{inh} values between chimeras and PI reflect distinct conformations of the contact residues. We specifically investigated the effect on k_{inh} values of the multiple Pro residues and the shorter length of the PI reactive loop, features unique to the PI loop that might be expected to play a major role in determining contact region structure. Incorporation of these features in the ACT−PI chimeras had surprisingly little effect on the

inhibition rates as k_{inh} values were essentially the same as the P6−P3′ region chimeras. Overall, the results of the reactive loop switching studies suggest that k_{inh} is not determined by reactive loop sequence alone. Lawrence and co-workers (*31*) reached a similar conclusion by studying reactive loop chimeras of PAI-1.

Comparison of the X-ray crystal structure of rACTcas−P3P3′ (*32*) with the recently solved crystal structure of an intact variant of recombinant PI (PI-F51L) (*33*) suggests a rationale for the differences in HNE inhibitory rate constants between PI and the ACT−PI chimeras. The P10−P3′ region of the reactive loop of rACTcas−P3P3′ assumes a distorted helical conformation. In contrast, the P8−P3′ region of PI-F51L adopts a β-strand conformation with the P3−P3′ residues essentially in the "canonical" proteinase-bound conformation. The observed loop structure for PI-F51L appears to be stabilized by several interactions between the reactive loop and body, the most notable of which is the interaction of the P5−Glu and a positively charged pocket on the underlying surface, a pocket that is absent in ACT. Therefore, while the reactive loop residues surrounding the scissile bond of PI are constrained in a conformation that is complementary to the substrate binding site of HNE, the reactive loop of the ACT−PI chimeras are not (*32*). The constraint of contact residues in a binding conformation might be expected to greatly enhance the rate of association between PI and HNE (*23*). Although another recent report (*34*) describing the X-ray crystal structure of a PI variant (hepta-PI) claims that the reactive loop adopts a distorted helix conformation, the structural differences described above for rACTcas−P3P3′ and PI-F51L do provide a compelling explanation for the inability of ACT−PI chimeras to reach the k_{inh} values demonstrated by PI.

Fluorescence, proton NMR, and protease susceptibility studies indicate that both the serpin (*5*−*8*, *11*) and protease (*9*, *10*, *35*−*37*) have altered conformations in the complex. Without high-resolution structural data describing a serpin−protease complex it is only possible to speculate on the contacts between serpins and proteases that stabilize the complex. The P6−P3′ series of ACT−PI chimeras form complexes with HNE that exhibit a broad range of k_{bkdn} values. These ACT−PI chimeras were not a series of defective serpins since rACT−P6P3′, the chimera that forms the least stable complexes with HNE, forms complexes with the chymotrypsin-like protease human chymase that do not significantly break down even after 24 h in 1 M NaCl (*38*). Therefore, analysis of the substitutions producing the range of k_{bkdn} values may reveal serpin structural elements involved in complex stabilization. In fact, the relatively dramatic effects on k_{bkdn} noted when the residues at the P1, P3, and/or P4 position were changed most likely reflects reactive loop−protease interactions and suggest that at least the P4−P1 residues of the contact region are involved in the stabilization of chimera−HNE complexes.

Although ACT−PI chimeras appeared to be fully functional serpins, chimera−HNE complexes never attained the full measure of stability observed for PI−HNE complexes. Furthermore, chimeras with the largest portions of the contact region of PI (rACT−P6P3′ and rACT−P4P3′) formed the least stable complexes with HNE. These results suggest that the reactive loop sequence alone does not determine complex stability. Instead, it is likely that complex stability also depends on interactions between the bodies of the serpin and protease. Serpin body−protease body interactions are suggested by modeling experiments (*39*−*41*) which predict that either partial or complete insertion of the reactive loop into the A-β-sheet brings the serpin and protease bodies into close proximity. Recent fluorescence resonance energy transfer experiments by Stratikos and Gettins (*42*) confirm that the formation of the stable complex is associated with a major translocation of the protease from its position in the initial encounter complex. Furthermore, work by Wilcznska et al. (*43*) utilizing both fluorescence resonance energy transfer and cross-linking reagents suggests that the complexed protease is held near the surface of the A-β-sheet and helix-F. Body−body contacts may provide the interactions that help distort the protease or limit the entry of solvent to the active site (*39*), thereby trapping the protease in a covalent complex. The inability of ACT−PI chimeras to form highly stable complexes with HNE may indicate the absence of the appropriate body−body contacts or the presence of unfavorable body−body interactions.

In contrast to the considerable changes in complex breakdown rates noted with the unprime side residue changes, k_{bkdn} was insensitive to changes on the prime side of the reactive loop. Even the deletion of the P6′−P9′ residues did not appear to affect complex breakdown. This suggests that the prime side residues of the loop play little role in complex stabilization. Such an interpretation is consistent with an acyl enzyme-type serpin−protease complex (*11*, *12*, *44*) where the P1−P1′ bond is cleaved and only unprime side residues of the reactive loop remain in contact with the protease.

In summary, we found that the inhibitory activity of PI against HNE could not be completely transferred to ACT through a loop-switching strategy. ACT−PI chimeras probably failed to attain the rapid HNE inhibition rates because the reactive loop of the chimeras could not recapitulate the structure of the PI loop. Furthermore, the ACT−PI chimeras probably formed relatively unstable complexes with HNE because of a "poor fit" between the ACT and HNE bodies. Overall, the results of the current study suggest that the serpin body may play an important role in determining both inhibition and complex breakdown rates for target proteases. Therefore, reactive loop−serpin body and serpin body−protease body interactions should be considered in efforts to design recombinant serpins with narrow target specificity and/or optimal inhibitory characteristics.

ACKNOWLEDGMENT

We appreciate the excellent technical assistance provided by the protein chemistry facility at the Wistar Institute (Philadelphia) which performed all the mass spectroscopic analyses. We thank Dr. Trevor Selwood for helpful discussions, and Michele Walter for help with the purification of recombinant serpins.

REFERENCES

1. Schechter, I., and Berger, A. (1967) *Biochem. Biophys. Res. Commun. 27*, 157−162.
2. Travis, J., and Salvessen, G. S. (1983) *Annu. Rev. Biochem. 52*, 655−709.
3. Mast, A. E., Enghild, J. J., Pizzo, S. V., and Salvesen, G. (1991) *Biochemistry 30*, 1723−1730.
4. Debrock, S., and Declerk, P. J. (1995) *FEBS Lett. 376*, 243−246.

5. Björk, I., Nordling, K., and Olson, S. T. (1993) *Biochemistry 32*, 6501−6505.
6. Shore, J. D., Day, D. E., Francis-Chmura, A. M., Verhamme, I., Kvassman, J., Lawrence, D. A., and Ginsburg, D. (1995) *J. Biol. Chem. 270*, 5395−5398.
7. Olson, S. T., Bock, P. E., Kvassman, J., Shore, J. D., Lawrence, D. A., Ginsburg, D., and Björk, I. (1995) *J. Biol. Chem. 270*, 30007−30017.
8. O'Malley, K. M., Nair, S. A., Rubin, H., and Cooperman, B. S. (1997) *J. Biol. Chem. 272*, 5354−5359.
9. Plotnick, M. I., Mayne, L., Schechter, N. M., and Rubin, H. (1996) *Biochemistry 35*, 7586−7590.
10. Kaslik, G., Kardos, J., Szabó, E., Szilágyi, L., Závodsky, P., Westler, W. M., Markley, J. L., and Gráf, L. (1997) *Biochemistry 36*, 5455−5464.
11. Lawrence, D. A., Ginsburg, D., Day, D. E., Berkenpas, M. B., Verhamme, I. M., Kvassman, J.-O., and Shore, J. D. (1995) *J. Biol. Chem. 270*, 25309−25312.
12. Wilcznska, M., Fa, M., Ohlsson, P.-I., and Ny, T. (1995) *J. Biol. Chem. 270*, 29652−29655.
13. Rubin, H., Plotnick, M., Wang, Z. M., Liu, X., Zhong, Q., Schechter, N. N., and Cooperman, B. S. (1994) *Biochemistry 33*, 7627−7633.
14. Bode, W., Edgar Meyer, J., and Powers, J. C. (1989) *Biochemistry 28*, 1951−1963.
15. Nakajima, K., Powers, J. C., Ashe, B. M., and Zimmerman, M. (1979) *J. Biol. Chem. 254*, 4027−4032.
16. Powers, J. C., Gupton, B. F., Harley, A. D., Nishino, N., and Whitley, R. J. (1977) *Biochem. Biophys. Acta 485*, 156−166.
17. Rubin, H., Wang, Z. M., Nickbarg, E. B., McLarney, S., Naidoo, N., Schoenberger, O. L., Johnson, J. L., and Cooperman, B. S. (1990) *J. Biol. Chem. 265*, 1199−1207.
18. Schonbaum, G. R., Zerner, B., and Bender, M. L. (1961) *J. Biol. Chem. 236*, 2930−2935.
19. Djie, M. Z., Bonniec, B. F. L., Hopkins, P. C. R., Hipler, K., and Stone, S. R. (1996) *Biochemistry 35*, 11461−11469.
20. Cooperman, B. S., Stavridi, E., Nickbarg, E., Rescorla, E., Schechter, N., and Rubin, H. (1993) *J. Biol. Chem. 268*, 23616−23625.
21. Schechter, N. M., Sprows, J. L., Schoenberger, O. L., Lazarus, G. S., Cooperman, B. S., and Rubin, H. (1989) *J. Biol. Chem. 264*, 21308−21315.
22. Waley, S. G. (1985) *Biochem. J. 227*, 843−849.
23. Gettins, P. G. W., Patston, P. A., and Olson, S. T. (1996) *Serpins: Structure, Function and Biology*, p 202, R. G. Landes Co., Austin, TX.
24. Madison, E. L., Goldsmith, E. J., Gething, M.-J. H., Sambrook, J. F., and Gerard, R. D. (1990) *J. Biol. Chem. 265*, 21423−21426.
25. Ehrlich, H. J., Gebbink, R. K., Keijer, J., Linders, M., Preissner, K. T., and Pannekoek, H. (1990) *J. Biol. Chem. 265*, 13029−13035.
26. York, J. D., Li, P., and Gardell, S. J. (1991) *J. Biol. Chem. 266*, 8495−8500.
27. Sherman, P. M., Lawrence, D. A., Verhamme I. M., Paielli, D., Olson, S. T., Shore, J. D., and Ginsburg, D. (1995) *J. Biol. Chem. 270*, 9301−9306.
28. Phillips, J. E., Cooper, S. T., Potter, E. E., and Church, F. C. (1994) *J. Biol. Chem. 269*, 16696−16700.
29. Theunissen, H. J. M., Dijkema, R., Grootenhuis, P. D. J., Swinkels, J. C., de Poorter, T. L., and Visser, P. C. a. A. (1993) *J. Biol. Chem. 268*, 9035−9040.
30. Hopkins, P. C., Crowther, D. C., Carrell, R. W., and Stone, S. R. (1995) *J. Biol. Chem. 270*, 11866−11871.
31. Lawrence, D. A., Strandberg, L., Ericson, J., and Ny, T. (1990) *J. Biol. Chem. 265*, 20293−20301.
32. Wei, A., Rubin, H., Cooperman, B. S., and Christianson, D. W. (1994) *Nature Struct. Biol. 1*, 251−258.
33. Elliot, P. R., Lomas, D. A., Carrell, R. W., and Abrahams, J. P. (1996) *Nature Struct. Biol. 3*, 676−681.
34. Ryu, S.-E., Choi, H.-J., Kwon, K.-S., Lee, N., and Yu, M.-H. (1996) *Structure 4*, 1181−1192.
35. Hervé, M., and Ghélis, C. (1991) *Arch. Biochem. Biophys. 285*, 142−146.
36. Kaslik, G., Patthy, A., Bálint, M., and Gráf, L. (1995) *FEBS Lett. 370*, 179−183.
37. Stavridi, E. S., O'Malley, K., Lukacs, C. M., Moore, W. T., Lambris, J. D., Christianson, D. W., Rubin, H., and Cooperman, B. S. (1996) *Biochemistry 35*, 10608−10615.
38. Schechter, N. M., Plotnick, M. I., Selwood, T., Walter, M., and Rubin, H. (1997) *J. Biol. Chem. 272*, 24499−24507.
39. Wright, H. T., and Scarsdale, J. N. (1995) *Proteins 22*, 210−225.
40. Whisstock, J., Lesk, A. M., and Carrell, R. (1996) *Proteins 26*, 288−303.
41. Aertgeerts, K., Ranter, C. J. D., Booth, N. A., and Declerk, P. J. (1997) *J. Struct. Biol. 118*, 236−242.
42. Stratikos, E., and Gettins, P. G. W. (1997) *Proc. Natl. Acad. Sci. U.S.A. 94*, 453−458.
43. Wilcznska, M., Fa, M., Karolin, J., Ohlsson, P.-I., Johansson, L. B.-Å., and Ny, T. (1997) *Nature Struct. Biol. 14*, 354−357.
44. Fa, M., Karolin, J., Aleshkoff, S., Strandberg, L., Johansson, L. B.-Å., and Ny, T. (1995) *Biochemistry 34*, 13833−13840.

BI971530J